ACS Catalysis

Research Article

pubs.acs.org/acscatalysis

DFT Modeling of the Aldehyde–Water Shift Reaction with a Cationic Cp*Ir Catalyst

William C. Ou and Thomas R. Cundari*

Department of Chemistry, Center for Advanced Scientific Computing and Modeling (CASCaM), CCI Center for Enabling New Technologies through Catalysis, University of North Texas, P.O. Box 305070, Denton, Texas 76203-5070, United States

ABSTRACT: Density functional theory calculations were used to assess the viability of an Ir^{III} complex, $Cp^*Ir^{III}(bpy\text{-}(OH)_2)(H_2O)[OTf]_2$, as a catalyst for the aldehyde–water shift (AWS) reaction ($R–CHO + H_2O \rightarrow R–COOH + H_2$), a reaction of considerable interest because of its potential implications for bulk hydrogen production and the "green" oxidation of aldehydes. Calculated thermodynamic and kinetic values for the steps in a proposed reaction mechanism with R = Me are reported. Calculations were conducted in both the gas phase and a continuum water solvent, with both sets of data showing similar energy trends. Overall, the data suggest that the Ir^{III} and related complexes are catalyst leads worthy of experimental consideration. The Rh^{III} and Ru^{II} variants of the proposed catalyst were also tested, and the following order of catalyst effectiveness was proposed: Rh > Ir > Ru. This order suggests that the Rh variant is also worthy of experimental testing.

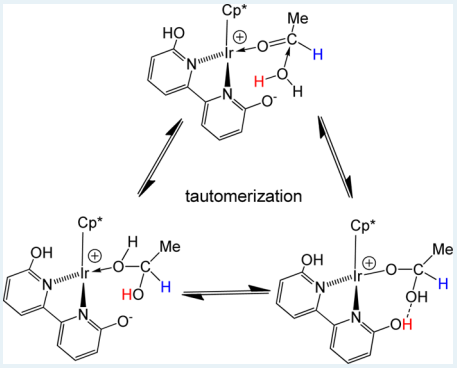

KEYWORDS: *aldehyde–water shift, density functional theory, green chemistry, aqueous catalysis, carboxylic acids*

I. INTRODUCTION

The aldehyde–water shift (AWS) reaction, the conversion of aldehydes and water to carboxylic acids and hydrogen gas (eq 1), was first reported by Murahashi et al.[1] and appeared again in the literature when Stanley et al. coined the name and reported the selective conversion of heptaldehyde to heptanoic acid with a CO-bridged dirhodium catalyst.[2,3]

$$R–CHO + H_2O \rightarrow R–COOH + H_2 \quad (1)$$

The aldehyde–water shift reaction is of considerable interest because of its potential applications to industrial hydrogen production and to hydrogen fuel cells. The aldehyde shift of formaldehyde to formic acid followed by the decomposition of formic acid to H_2 and CO_2 would result in 2 moles of H_2 being produced for every mole of formaldehyde consumed (8.3% by weight). The AWS uses water as a hydrogen source as opposed to the hydrocarbon sources currently utilized in bulk hydrogen production. The use of water as a renewable hydrogen source has substantial precedent because various electrolytic[4] and thermolytic[5] processes have been extensively studied. However, the AWS offers benefits in that it does not require large amounts of energy or heat to be carried out, a trait shared only by processes that utilize light energy.[6] Finally, carboxylic acids (R–COOH) and compounds derived from them also have applications in industry, and although many methods of producing carboxylic acids from aldehydes require potent oxidizing reagents,[7] the AWS does not.

Later reports by Stanley's group detail an AWS mechanism, similar to that of Murahashi et al.,[1] using their proposed dirhodium catalyst.[3] The mechanism begins with nucleophilic attack on the ligated aldehyde by water, followed by the loss of a proton from the aldehyde hydrate and β-hydride elimination, yielding the carboxylic acid complex. Dissociation of the carboxylic acid, protonation of the hydride, and finally H_2 loss close the catalytic cycle. One point of note is that Stanley et al. proposed that a bimetallic assembly was critical to the AWS reaction via controlling the Lewis acidity (i.e., the energy of the lowest unoccupied molecular orbital) through the combined cationic effects of the metals and through the stabilizing effects of the bridging CO ligands.[2,3] However, Murahashi's catalyst was a monometallic Ru system,[1] and the proposed catalytic steps summarized above occur at a single metal. Thus, the possibility of a single metal catalyst remains worthy of computational investigation.

Despite its potential significance, the aldehyde–water shift has remained largely unexplored. However, Rodríguez-Lugo et al. have recently reported the successful synthesis of a Rh system that catalyzes the conversion of methanol and water mixtures to CO_2/H_2 gas via an experimentally supported mechanism with significant ligand involvement.[8] This mechanism includes the AWS as an intermediate step, supporting the above-stated idea that it is likely possible to perform aldehyde–water shift catalysis using a monometallic system and suggesting that systems involving metal–ligand cooperation should be considered. The purpose of this study was to identify and model potential catalysts for the AWS reaction.

On the basis of computational and experimental precedents outlined in a recent communication by our group,[9] we

Received: August 19, 2014
Revised: October 23, 2014
Published: November 17, 2014

identified $Cp^*Ir^{III}(bpy{-}(OH)_2)(H_2O)^{2+}$ ($Cp^* = \eta^5\text{-}C_5Me_5$), complex **1**, as a catalyst lead for the aldehyde–water shift (Figure 1). Kawahara et al. found that **1** is capable of catalyzing

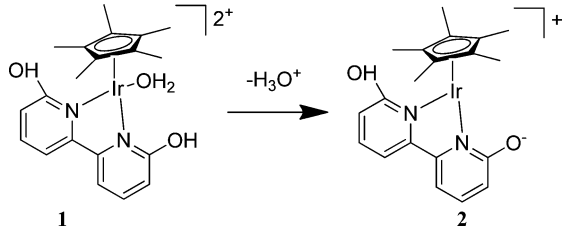

Figure 1. Proposed catalyst for the aldehyde–water shift reaction. Elimination of H_3O^+ from **1** yields **2**, which is the starting point of the modeled catalytic cycle. Previous studies show that the presence of OTf^- as the counteranion species resulted in a higher catalytic activity compared to that in the presence of PF_6^- and BF_4^-.[10]

the oxidative dehydrogenation of alcohols, proposing a mechanism in which both metal and ligand play a significant role.[10] Dicationic **1** is first converted to monocationic, unsaturated species $Cp^*Ir(bpy{-}OH,O^-)^+$, **2**. The latter is the starting point for the proposed reaction pathway, which involves the coordination of an alcohol, the transfer of H^+ to the diimine ligand, and β-hydride elimination of the resulting alkoxo moiety to form an Ir^{III}–hydrido complex, from which dihydrogen is lost via reaction of the hydride ligand with the hydroxyl proton of the functional ligand.[10]

The dehydrogenation mechanism proposed by Kawahara et al. is quite similar to Stanley's proposed AWS mechanism,[3] giving rise to the possibility that the AWS could be easily adapted to catalyst complex **1**. Furthermore, complex **1** is water-soluble,[10] which is desirable both because water is a reactant and because water as a solvent is extremely attractive from the standpoint of green chemistry principles.[11] Finally, it has been recently reported that a very closely related Cp*Ir complex is capable of catalyzing the disproportionation of formic acid into methanol, suggesting that **1** could be used to produce methanol from formaldehyde via a tandem reaction.[12] For these reasons, an investigation of the possibility of using **1** as the basis for an AWS catalyst was conducted. DFT calculations were carried out using **1** to model the conversion of acetaldehyde to acetic acid[21] (R = Me in eq 1) via the aldehyde–water shift reaction to assess the viability of this complex and related complexes as proposed AWS catalysts and to delineate the energetics of critical steps in a putative catalytic cycle.

II. COMPUTATIONAL METHODS

All density functional theory (DFT) calculations were made with the Gaussian 09[13] package using the PBE0 (PBE1PBE) hybrid functional.[14] Iridium was modeled with the SDD pseudopotential (60-electron core),[15] and its attendant valence basis set was augmented with a single f-polarization function with an exponent of 0.685. Main group elements were modeled with the 6-311G** all-electron basis set.[16] This level of theory was used in a recent computational study of iridium-mediated C–H bond activation and produced results that were consistent with experimental energetics.[17] Unless otherwise noted, calculations were conducted in the gas phase at 298.15 K and 1 atm. Solvent calculations were performed in water solvent using the SMD solvation model.[18] All calculated free energies are reported in kcal mol^{-1}. Optimized ground states contained zero imaginary vibrational frequencies, and optimized transition states contained exactly one imaginary vibrational frequency.

III. RESULTS AND DISCUSSION

A. Mechanism. The proposed mechanism in Scheme 1 for the aldehyde–water shift with catalyst **1** is based on the

Scheme 1. Mechanism for the Aldehyde–Water Shift with Proposed Catalyst 2[a]

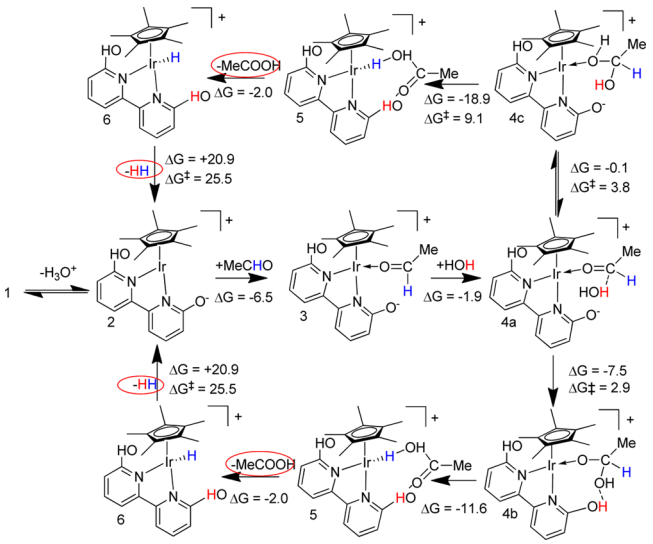

[a]PBE1PBE/SDD/6-311G**-calculated ΔG (kcal mol^{-1}) values for each step in the mechanism are also reported along with calculated $\Delta G^{\ddagger}$ values (kcal mol^{-1}).

mechanistic proposals made by our group,[9] the Stanley group,[2,3] and Kawahara et al.[10] Additionally, recent DFT studies of acceptorless alcohol dehydrogenation by Li and Hall[19] provided value guidance for the proposed mechanism of AWS catalysis. The elimination of H_3O^+ from **1** yields 16-electron species **2**, with a single vacant coordination site. Using hydronium/water to model a conjugate acid/base pair in conjunction with a continuum water solvent model (SMD[18]), reaction **1** → **2** is endergonic by 13 kcal/mol. With an improved conjugate acid/base pair model (eigencation ($H_9O_4^+$)/water tetramer), the reaction is ostensibly thermoneutral ($\Delta G = -1$ kcal/mol) in SMD water. At this point, MeCHO coordinates to Ir, forming **3**. The κ^1-O linkage isomer is computed to be the preferred ligation mode of acetaldehyde in **3**. Next, a weak donor–acceptor interaction between the O of H_2O and the carbonyl C of the aldehyde leads to species **4a**, the hydrate tautomer. The modeled cycle then branches into one of two pathways. In the first, nucleophilic attack by H_2O and the simultaneous migration of a water proton to the O^- of the diimine ligand forms "deprotonated" tautomer **4b**, which is stabilized by two hydrogen bonds between the hydroxyl groups of the diimine and the oxygens of the deprotonated hydrate ligand. This species undergoes β-hydride elimination, forming species **5**, the acetic acid complex. In the second pathway, **4a** undergoes tautomerization to form **4c**, termed the "diol" tautomer. The complex is stabilized by a hydrogen bond to the diimine ligand. Next, in a Noyori-style mechanism,[20] H^+ and H^- are simultaneously transferred to the diimine and metal, respectively, producing **5**. In species **5**, acetic acid is no longer coordinated to the metal but is instead stabilized by an H-bond

dx.doi.org/10.1021/cs501222m | ACS Catal. 2015, 5, 225–232

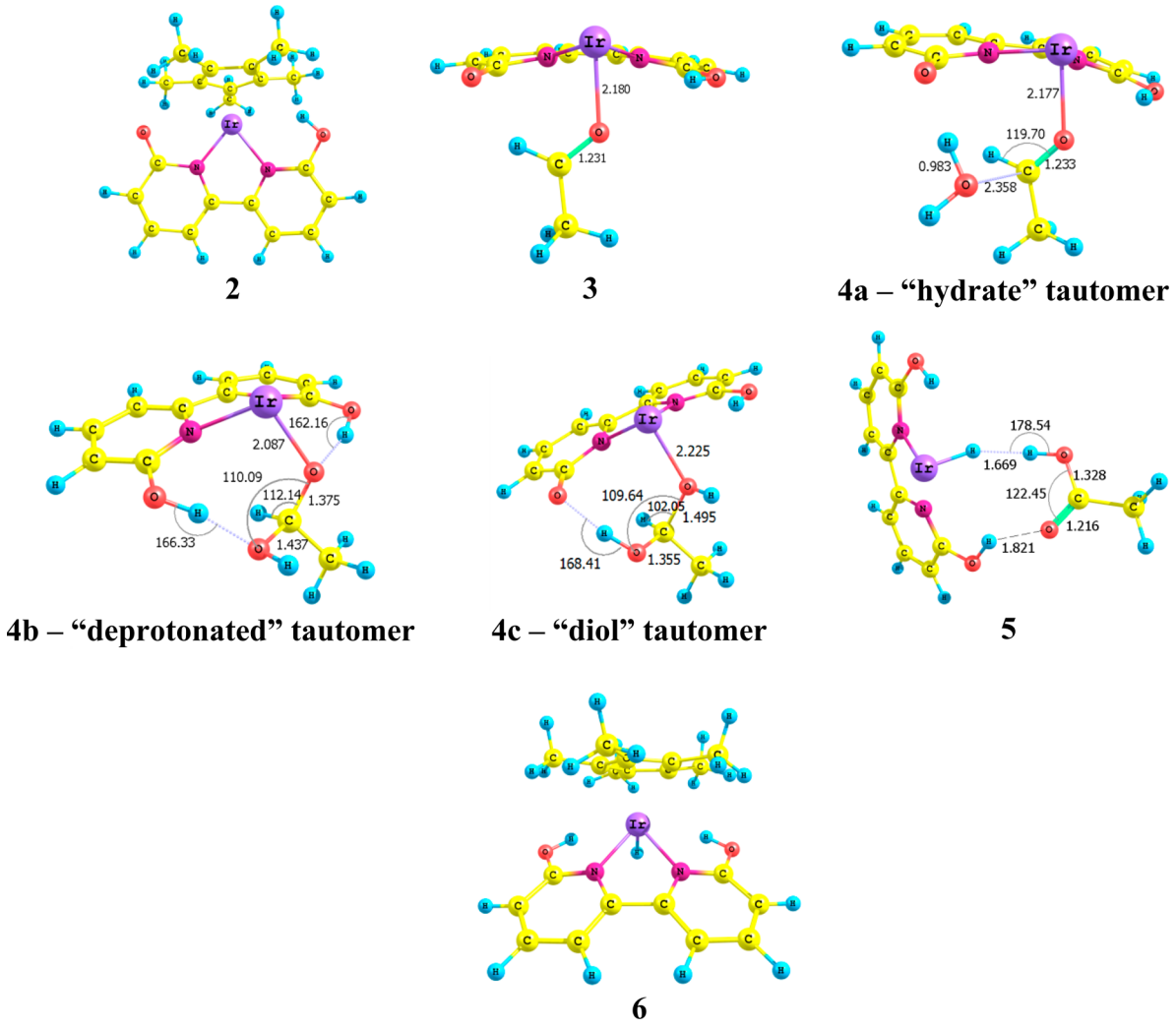

Figure 2. Optimized ground states for each intermediate in the proposed catalytic cycle in Scheme 2. Bond lengths (angstroms) and angles (degrees) of interest are labeled. Conformers with diimine OH components turned outward, away from Ir, were calculated to be higher in energy. Hydrogen bonding in complex **4b** stabilizes the structure and lowers the energy. Cp* id omitted in **3**–**5** for clarity.

between the acetic acid hydroxyl group and the hydride ligand.[22] Acetic acid then dissociates, forming species **6**. Finally, the transferred hydride on the metal reacts with the proton on the diimine ligand, and H_2 is released, reforming species **2** and closing the catalytic cycle. Optimized ground states for structures **2**–**6** are shown in Figure 2 along with pertinent bond angles and lengths. Scheme 1 also shows the energetics for the steps in the reaction mechanism; these will be discussed below.

As noted above, a key point in the proposed AWS mechanism is the existence of two possible reaction pathways revolving around three tautomers of the aldehyde hydrate (hydrate **4a**, deprotonated tautomer **4b**, and diol **4c**), all of which can interconvert. Scheme 2 shows all three tautomers and the respective ΔG and $\Delta G^{\ddagger}$ values of tautomerization relative to hydrate tautomer **4a**. In the gas phase, deprotonated structure **4b** is significantly more stable than the other tautomers and is therefore the most likely thermodynamically. (Note that in section D, computations indicate that in continuum water solvent, **4c** is the most thermodynamically stable of the three tautomers.) Assuming that water solvent calculations provide a more accurate picture of the behavior of the system in an experimental setting, we suggest that the

Scheme 2. Three Tautomers That Can Exist upon Hydration of Acetaldehyde[a]

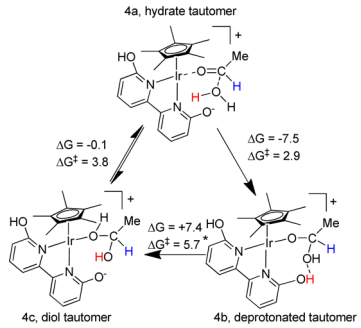

[a]PBE1PBE/SDD/6-311G**-calculated ΔG values (kcal mol^{-1}) for tautomerization (from **4a**) are also shown along with calculated $\Delta G^{\ddagger}$ values (kcal mol^{-1}). * = Gibbs free energy of the transition state estimated using polarizable continuum solvation model (PCM) optimized geometry.

pathway involving **4c** is favored over the **4b** pathway in Scheme 1. However, given the level of uncertainty in the DFT models, the **4b** pathway cannot be ruled out entirely. In terms of

dx.doi.org/10.1021/cs501222m | ACS Catal. 2015, 5, 225–232

kinetics, both tautomerization reactions have relatively mild barriers, indicating that there are no major kinetic roadblocks to any of these transformations.

In closing this section, we note that the possibility of reversing the original mechanism and transferring a hydride first, rather than a proton, was also considered. All calculations run to test this hypothesis resulted in geometries that were much higher in energy than those stationary points depicted in the mechanism in Scheme 1 or in geometries that failed to optimize, suggesting that these structures are very unstable and are unlikely to exist. Furthermore, because the hydride is transferred internally and because charge must be conserved, the hydrated aldehyde would have to be a cationic ligand, an unlikely scenario. Therefore, we ruled out this possibility and, by extension, the possibility of Ir^{V} species being involved in the reaction. Other simulations also suggests that Ir^{I} intermediates were likewise high in free energy. Therefore, in all low-energy species it has been assumed that Ir maintains a formal oxidation state of 3+ throughout the AWS catalytic cycle.

B. Reaction Thermodynamics. Calculations indicate that the thermodynamics of the **1**-catalyzed AWS are favorable. The coordination of MeCHO (**2** → **3**, ΔG = −6.5 kcal mol^{-1}), hydration (**3** → **4a**, ΔG = −1.9 kcal mol^{-1}), both tautomerization reactions (**4a** → **4b**, ΔG = −7.5 kcal mol^{-1}; **4a** → **4c**, ΔG = −0.1 kcal mol^{-1}), β-hydride elimination (**4b** → **5**, ΔG = −11.6), simultaneous H^+/H^- transfer (**4c** → **5**, ΔG = −18.9), and the elimination of acetic acid (**5** → **6**, ΔG = −2.0) are exergonic (Scheme 1). The calculated total ΔG of the catalytic cycle is −8.5 kcal mol^{-1}, and the calculated ΔG_{rxn} (**3** + H_2O → **5**) is −20.9 kcal mol^{-1}, which is more exergonic than the calculated ΔG_{rxn} for the AWS reaction without the Cp*Ir catalyst, −8.5 kcal mol^{-1}. The metal-free ΔG_{rxn} value is in good agreement with the value calculated by Stanley et al. (−28.4 kJ mol^{-1} = −6.8 kcal mol^{-1}).[2] The elimination of H_2 (**5** → **6**, ΔG = +20.9) was the only step computed to be endergonic within the reaction pathway (Scheme 1).

Table 1 compares the calculated ΔG values for the reaction steps outlined in Scheme 1 to calculated values for the analogous steps without any catalyst. Hydration and proton loss/transfer become more thermodynamically favored with the catalyst model, and hydride loss and simultaneous transfer become less favored but still remain downhill.

Table 1. PBE1PBE/SDD60/6-311G-Calculated ΔG Values (kcal mol^{-1}) for Hydration, Proton Loss/Tautomerization, and Hydride Loss/β-Hydride Elimination for MeCHO, with and without the Cp*Ir(diimine) Catalyst[a]**

step	without Cp*Ir	with Cp*Ir
3 → **4a** (hydration of aldehyde)	−0.8	−1.9
4a → **4b** (tautomerization/proton transfer to diimine)	+148.5	−7.5
4b → **5** (β-hydride elimination)	−157.9	−11.6
4c → **5** (simultaneous H^+/H^- transfer)	−25.9	−18.9

[a]Metal-free calculations use the water tetramer as the base.

C. Reaction Barriers. DFT modeling of the kinetics of the modeled AWS catalytic cycle also resulted in favorable findings. Optimized tautomerization transition states, (**4a**−**4b**)‡, (**4a**−**4c**)‡, and (**4b**−**4c**)‡, are shown in Figure 3 along with the calculated gas-phase barriers that are 2.9, 3.8, and 5.7 kcal mol^{-1}, respectively. Thus, barriers for all three of these

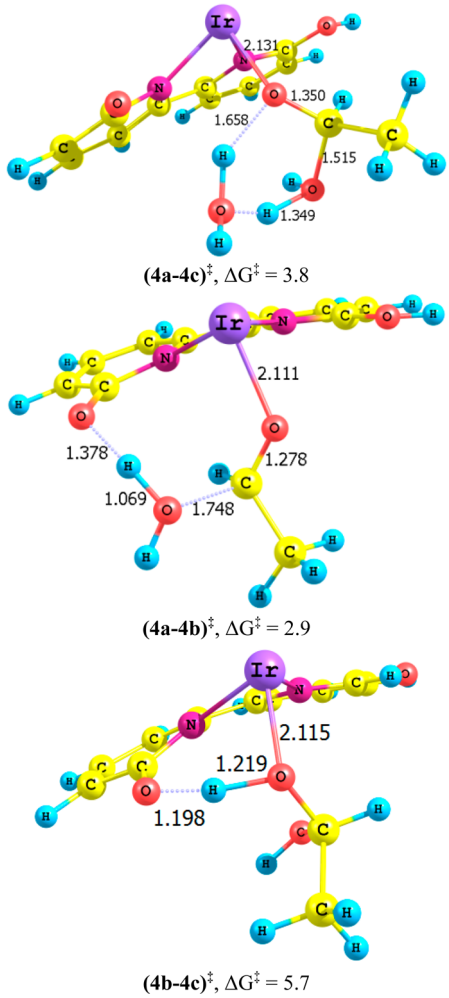

Figure 3. Transition states for the tautomerization reactions shown in Scheme 2. PBE1PBE/SDD/6-311G**-calculated $\Delta G^{‡}$ values (kcal mol^{-1}) for each reaction is also reported. As shown in (**4a**−**4c**)‡, conversion from **4a** to **4c** involves the addition of a second water molecule to form a 6-membered ring. (**4a**−**4b**)‡ shows simultaneous nucleophilic attack and proton transfer. Cp* is omitted for clarity.

tautomerizations are extremely low, implying that tautomerization is quite facile in all of these cases. Therefore, as stated above, calculated kinetic quantities do not significantly favor any one tautomer over the others.

Figure 4 shows the optimized transition state for simultaneous H^+/H^- loss from the diol complex, (**4c**−**5**)‡. The calculated barrier is 9.1 kcal mol^{-1}, which is reasonably low. Thus, both thermodynamic and kinetic calculations suggest that this step occurs quite readily.

The optimized transition state for H_2 loss, (**5**−**6**)‡ is shown in Figure 5. The calculated barrier for this step is 25.5 kcal mol^{-1}. As such, this represents the largest computed barrier in the proposed catalytic cycle in Scheme 1. Despite numerous attempts, an optimized β-hydride elimination transition state for the transformation of **4b** to **5** could not be located. Its relevance may be muted, however, in light of the proposition that the alternative, Noyori-like simultaneous H_2 transfer pathway is more likely.

D. Solvent Calculations. As stated above, the proposed catalyst precursor, **1**, is water-soluble.[10] Therefore, in addition to gas-phase calculations, water solvent calculations were performed in order to model the AWS under more realistic

dx.doi.org/10.1021/cs501222m | ACS Catal. 2015, 5, 225−232

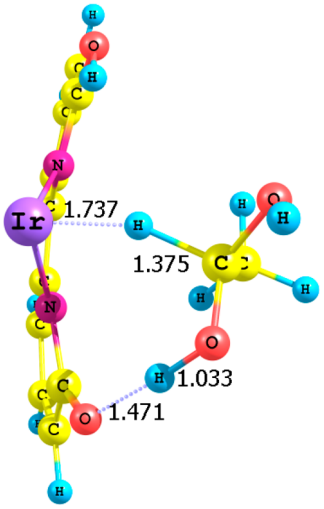

(4c-5)‡, $\Delta G^{‡}$ = 9.1

Figure 4. Transition state for H^+/H^- loss from **4c** to form **5**. PBE1PBE/SDD/6-311G**-calculated $\Delta G^{‡}$ is also reported (kcal mol^{-1}). Iridium accepts the hydride, and the diimine oxygen accepts the proton. Cp* is omitted for clarity.

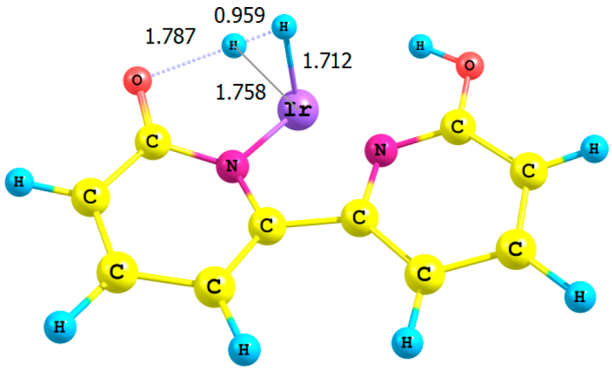

(6-2)‡, $\Delta G^{‡}$ = 25.5

Figure 5. Transition state for the H_2 loss step. PBE1PBE/SDD/6-311G**-calculated $\Delta G^{‡}$ is also reported (kcal mol^{-1}). The metal hydride reacts with one of the diimine hydroxyl protons, resulting in the release of H_2. Cp* is omitted for clarity.

aqueous conditions. The mechanism modeled was identical to the above-discussed mechanism based on gas-phase data. Tables 2 and 3 compare solvent and gas-phase calculated ΔG and $\Delta G^{‡}$ values for the individual steps in the reaction mechanism.

Table 2. PBE1PBE/SDD/6-311G-Calculated ΔG Values for Each Step in the Proposed Reaction Mechanism**[a]

step	gas phase	water solvent
2 + MeCHO→ **3**	−6.5	+6.0
3 + H_2O → **4a**	−1.9	+2.9
4a → **4b**	−7.5	−2.0
4b → **5**	−11.6	−9.8
4a → **4c**	−0.1	−6.1
4c → **5**	−18.9	−5.8
5 → **6** + MeCOOH	−2.0	−5.6
6 → **2** + H_2	+20.9	+6.9

[a]Both gas-phase and water solvent calculated values are shown.

Table 3. PBE1PBE/SDD/6-311G-Calculated $\Delta G^{‡}$ Values for Each Step in the Proposed Reaction Mechanism**[a]

step	gas phase	water solvent
(**4a**−**4b**)‡	2.9	7.8
(**4a**−**4c**)‡	3.8	12.6
(**4b**−**4c**)‡	5.7	1.2*
(**4c**−**5**)‡	9.1	16.7
(**6**−**2**)‡	25.5	18.9

[a]Both gas-phase and water solvent calculated values are shown. * = Gibbs free energy of the transition state estimated using polarizable continuum solvation model (PCM) optimized geometry.

With regard to calculated ΔG values, there does not seem to be an obvious linear correlation between the gas-phase and water solvent calculated values. Aldehyde coordination and hydration were calculated to be endergonic with the water solvent, although they remain close to thermoneutral. Another point of note is that the water solvent calculated ΔG values are generally more thermoneutral than their gas-phase counterparts, particularly in steps such as simultaneous H^+/H^- transfer (**4c** → **5**) and H_2 loss (**6** → **2** + H_2). Therefore, the continuum water simulations further bolster the plausibility of **1** as an AWS catalyst candidate and of the proposed mechanism summarized in Scheme 1.

The calculated barriers for hydrate−diol tautomerization (**4a** → **4c**) and simultaneous H_2 transfer (**4c** → **5**) are higher in the continuum water solvent than those obtained in the gas phase, but they remain relatively low (Table 3.) In addition, the most significant barrier in the gas phase, the H_2 loss barrier, was reduced from 25.5 to 18.9 kcal mol^{-1}. Thus, solvent calculations suggest that this H_2 loss step may be both more thermodynamically and kinetically favorable than previously thought, although it is still the most difficult step. Overall, the solvent data exhibit the same patterns that the gas-phase data do, being mostly exergonic with relatively mild barriers.

E. Catalyst Variants. Calculations modeling the proposed mechanism for the AWS with catalyst **1** indicated that most of the steps in the mechanism are exergonic and that the calculated barriers are all reasonable in magnitude, consistent with experimental observations.[9] Similar trends were seen in continuum aqueous solution models; reactions are generally closer to thermoneutral, and the "difficult" H_2 loss barrier is lower than in the gas-phase simulations. Thus, the proposed catalyst and reaction mechanism continue to be promising, prompting the consideration of several variants of complex **2** in order to assess the impact of the metal and ligand on the various steps in the reaction. For the sake of simplicity, a majority of these simulations were performed in the gas phase.

The first catalyst variant tested was complex **7**, in which the Ir of **2** is replaced by Rh, which belongs to the same group as Ir and which was the metal used by Stanley et al. in their experimental work (Figure 6).[2] The second catalyst variant, also shown in Figure 6, was complex **8**, in which the Ir is replaced by Ru and the Cp* ligand is replaced by Bz* (Bz* = η^6-C_6Me_6). The mechanisms modeled for the AWS with **7** and **8** are identical to the proposed Cp*Ir mechanism shown in Scheme 1. Tables 4 and 5 show comparisons of calculated ΔG and $\Delta G^{‡}$ values, respectively, among the three catalyst species.

As expected, the calculated thermodynamic values for group 9 complexes **2** and **7** are quite similar, with the largest differences occurring at the more thermodynamically extreme steps: both pathways for the formation of hydride−acetic acid

dx.doi.org/10.1021/cs501222m | ACS Catal. 2015, 5, 225−232

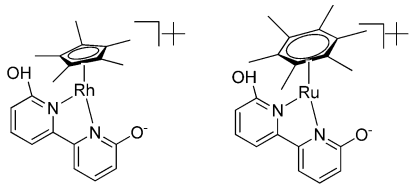

7 8

Figure 6. Variations on the proposed catalyst for the aldehyde–water shift. In **7**, the metal of **2** is replaced, with Rh being substituted for Ir. In **8**, both the metal and supporting ligand of **2** are replaced, with Ru replacing Ir and Bz* replacing Cp*.

Table 4. PBE1PBE/SDD/6-311G-Calculated ΔG Values for Each Step in the Proposed Reaction Mechanism with Catalyst Complexes 2, 7, and 8[a]**

step	gas-phase Cp*Ir (**2**)	water solvent Cp*Ir (**2**)	Cp*Rh (**7**)	Bz*Ru (**8**)
2 + MeCHO → **3**	−6.5	+6.0	−7.8	−17.8
3 + H_2O → **4a**	−1.9	+2.9	−2.3	−3.7
4a → **4b**	−7.5	−2.0	−6.0	−5.3
4b → **5**	−11.6	−9.8	−8.4	−7.8
4a → **4c**	−0.1	−6.1	−0.4	+0.2
4c → **5**	−18.9	−5.8	−14.0	−13.4
5 → **6** + MeCOOH	−2.0	−5.6	−0.01	−0.8
6 → **2** + H_2	+20.9	+6.9	+15.9	+24.0

[a]Steps are listed in terms of the Cp*Ir mechanism shown in Scheme 1. The other three species follow analogous pathways.

Table 5. PBE1PBE/SDD/6-311G-Calculated $\Delta G^{\ddagger}$ Values for Each Step in the Proposed Reaction Mechanism with Catalyst Complexes 2, 7, and 8[a]**

step	Cp*Ir (**2**)	Cp*Rh (**7**)	Bz*Ru (**8**)
(**4a**–**4b**)‡	2.9	2.5	3.7
(**4a**–**4c**)‡	3.8	2.3	5.3
(**4b**–**4c**)‡	5.7	4.9	4.7
(**4c**–**5**)‡	9.1	10.9	16.8
(**6**–**2**)‡	25.5	22.8	20.0

[a]Steps are listed in terms of the Cp*Ir mechanism shown in Scheme 1. The other three species follow analogous pathways.

adduct **5** and the H_2 loss step (**6** → **2** + H_2). Because both of these steps involve the metal, which is the only difference between the two complexes, such findings are reasonable. In all of these cases, the values for **7** are all closer to thermoneutral than are those of **2**, suggesting that rhodium complex **7** is also a worthy catalyst for further experimental study. Compared to Cp*Ir, the values for Ru^{II} complex **8** are more divergent for steps at the beginning and end of the catalytic cycle, and they become more thermoneutral in the middle of the model catalytic cycle. The most significant difference is in the MeCHO coordination, which becomes much more downhill. This suggests that this system is comparatively less stable in a 16-electron state, although it is unclear whether this is due to the effects of the Ru metal or the Bz* supporting ligand. The instability of the 16-electron system is an undesirable characteristic because it will likely become harder to perform the initial step in which this species is generated from the 18-electron catalyst in addition to reducing the favorability of the H_2 loss step. Another point of interest in the data for **8** is the fact that tautomerization from **4a** to **4c** becomes very slightly endergonic, meaning that the pathway involving **4c** is probably less likely to occur in comparison to the group 9 model systems.

As with the ΔG values, the calculated barriers for complexes **2** and **7** are quite similar (Table 5), again likely because of the fact that both are group 9 systems. In general, **7** has lower barriers than **2**, further contributing to its case as a candidate for additional investigation. This includes the H_2 loss barrier, which is ∼3 kcal mol^{-1} lower in the rhodium species than in the iridium species. Compared to the other two systems, complex **8** has higher barriers than the other two systems for two of the tautomerization reactions (**4a**–**4b** and **4a**–**4c**) and for simultaneous hydrogen transfer, whereas the barrier for H_2 loss is several kcal mol^{-1} lower. The barrier for the **4b**–**4c** transformation is also lower, although this transformation is not as relevant as the other two tautomerization reactions in the proposed reaction mechanism.

Overall, calculated thermodynamic and kinetic values suggest the order Cp*Rh > Cp*Ir > Bz*Ru for relative metal–ligand cooperative catalyst effectiveness.

IV. SUMMARY AND CONCLUSIONS

DFT calculations were performed to assess the viability of a proposed catalyst for the aldehyde–water shift reaction, $[Cp^*Ir(bpy\text{-}(OH)_2)(H_2O)]^{2+}$ (**1**), and a mechanism for the reaction involving both metal and ligand was proposed (Scheme 1). The free energy (ΔG) was calculated for each step using optimized ground states, and a majority of the steps were found to be thermodynamically downhill. Most importantly, H^+ transfer during tautomerization was found to be exergonic for the Cp*Ir system. This presumably eliminates the need for the very strong bases that might be necessary with other systems. The lone computed endergonic step is H_2 loss, and for this, an Rh variant of the Cp*Ir catalyst was found to be less endergonic, perhaps implying that the hydricity[9] of the metal complex is a key factor in catalyst activity. Transition states were also found for steps in the proposed mechanism, and the free-energy barriers ($\Delta G^{\ddagger}$) were calculated to be reasonable. Thus, we hypothesize that the entire reaction will remain quite facile throughout.

The AWS was also modeled with continuum water solvent calculations in order to evaluate the catalyst under more realistic conditions. The aldehyde coordination and hydration became slightly endergonic in water solvent, but overall, the calculated water ΔG values remained similar to their gas-phase counterparts, with the added benefit of generally being closer to thermoneutral. Additionally, the H_2 elimination step, the most difficult step in the gas-phase models kinetically and thermodynamically, was reduced in free-energy barrier and became less endergonic, respectively, upon the introduction of the continuum solvent model.

It is further noted that the present calculations provide support for the claims that the AWS reaction can be catalyzed by a monometallic system. We originally hypothesized that because metal–ligand cooperation plays an important role in the reaction pathway, perhaps in the absence of a cooperative ligand, two metals are needed to effect the disparate jobs of H^+ and H^- removal from the aldehyde hydrate substrate. This would also have been consistent with the observation by Yamaguchi and co-workers that showed a difference in reactivity between 4,4′-OH– and 6,6′-OH–bpy ligated catalysts.[10] The former presumably cannot participate in the deprotonation of the aldehyde hydrate.

dx.doi.org/10.1021/cs501222m | ACS Catal. 2015, 5, 225–232

Taken together, the present results, in conjunction with recent research,[9] indicate reasonable thermodynamics and kinetics for steps in a plausible mechanism for aldehyde−water shift catalysis.[9] Although more work is needed, experimentally and computationally, to deconvolute the AWS mechanism, computations suggest that other d^6 metals (e.g., Ru^{II} and Rh^{III}) are worthy of experimental scrutiny. In a recent joint theory−experiment study, $Cp^*Ir^{III}(bpy)$ and $Bz^*Ru^{II}(bpy)$ precatalysts were compared for AWS reactivity with an acetaldehyde substrate.[9] Ir^{III} precatalysts were generally more active for AWS whereas Ru^{II} precatalysts were more selective for the carboxylic acid product. Computed reaction free energies (Table 4) and free-energy barriers (Table 5) are generally within ±2 to 3 kcal/mol for Ir and Ru models. The most noticeable differences between these two metals are the much stronger binding of MeCHO to the Ru^{II} complex and the differences in computed thermodynamics and kinetics of H^+/H^- loss (e.g., **4c** → **5**) to form acetic acid from the aldehyde hydrate. The latter is computed to be less exergonic ($\Delta\Delta G \approx 51/2$ kcal/mol) and to possess a higher barrier ($\Delta\Delta G^{\ddagger} \approx 8$ kcal/mol) for this step for the Ru^{II} (**8**) versus Ir^{III} (**2**) complex. Although acetaldehyde was not studied experimentally[9] for Rh^{III} precatalysts with a propionaldehyde substrate, Rh^{III} congeners are less active and more selective than their Ir^{III} analogues. As with the ruthenium/iridium comparison, the H^+/H^- transfer step is less exergonic ($\Delta\Delta G \approx 5$ kcal/mol) and has a higher barrier ($\Delta\Delta G^{\ddagger} \approx 2$ kcal/mol) for the less active and more selective rhodium(III). Thus, the present work, in conjunction with experiments,[9] implicates hydrogen transfer as another key step in AWS catalysts. Given that the H_2 loss step (e.g., **6** → **2** + H_2) is also computed to be kinetically and thermodynamically demanding, one may surmise that the metal's hydricity is an important metric in the design of AWS catalysts moving forward.

Looking more closely at the transition-state geometry for the **4c** → **5** transformation (Figure 4) reveals two particularly relevant observations vis-à-vis AWS catalysis. First, the TS entails the dissociation of a ligated OH group in order to put the C−H bond from which the "hydride" is abstracted in the vicinity of the metal. Hasanayn and co-workers have discussed the importance of this catalyst/substrate separation in the context of the hydrogenation of dimethyl carbonate and esters by Ru−pincer complexes.[23,24] In those cases, dissociation entailed the formation of an anionic substrate and thus the formation of an ion pair. Of course, it is possible that in the case of AWS that the deprotonation of the diol substrate by an O^- on the diimine to yield a diolate could precede (and indeed even enhance) hydride transfer. Hasanayn and co-workers[23,24] have shown ion-pair and metal−ligand cooperative pathways to be similar in energy, with the former being lower in free energy for their metal/ligand/substrate combination. Similar TSs were sought in this work but repeatedly collapsed to transition states such as that depicted in Figure 4. A second interesting point with regard to $(\mathbf{4c}-\mathbf{5})^{\ddagger}$ is the synchronization of the H^+ and H^- transfers to the ligand and metal, respectively. The Ir−H distance is computed to be ∼1.7 Å, 0.1 Å longer than this bond in hydride product **5**. However, C−H ≈ 1.4 in this TS, which is ca. 30% longer than a typical carbon−hydrogen single bond. For the proton transfer, O−H ≈ 1.5 Å, a 50% lengthening versus a typical covalent bond value, and the O−H bond to the substrate that is being broken is 1.0 Å, or less than 10% lengthened as compared to the same bond in the diol ground state. Hence, the metric data is inconclusive as to the timing of the extent to which proton/hydride transfer is synchronized in $(\mathbf{4c}-\mathbf{5})^{\ddagger}$. Although computed atomic charges are complicated by the inherent approximations arising from partitioning the total electron density, they are interesting when comparing related hydrogen atoms in $(\mathbf{4c}-\mathbf{5})^{\ddagger}$. The proton being transferred has a Mulliken charge of $+0.36e^-$, which is marginally more positive than the spectator protons of the OH groups on the substrate ($+0.28e^-$) and supporting ligand ($+0.30e^-$). The hydride of the substrate that is being transferred is less positive compared to the spectator H on the methyl group of the substrate (+0.12 vs $+0.18e^-$).

The research described herein also suggests that further improvements in AWS catalysis may be obtainable through the judicious exploitation of metal−ligand cooperativity. As alluded to above, experiments by Kawahara et al. show a clear benefit upon going from bpy to 6,6′-OH−bpy (bpy−OH) for a related reaction with a similar proposed mechanism,[10] thus supporting metal−ligand cooperativity; this trend is less clear in experiments on AWS catalysts.[9] For example, the activity more than doubles from 16% to 39% conversion for Rh(bpy) versus Rh(bpy−OH) catalysts, but remains high for Ir variants (99% conversion for both supporting ligands) and low for Ru variants (5% and 6% conversion for bpy and bpy−OH, respectively).[9] An electronic origin may also be proposed given the π-donor/σ-withdrawing nature of OH functional groups, although in the case of Rh^{III} precatalysts, 4,4′-OMe-bpy was as active as the parent bpy (16% versus 17% conversion, respectively), and hence both are roughly half the activity of the bpy−OH ligated precatalyst. For Ir^{III} and Ru^{II}, the three diimine The work of Papish et al.[25] beautifully highlights the impact of pH and protonation state of bpy−OH ligands on their activity for transfer hydrogenation, ligands had the same activity as measured by conversion percentages. Hence, future AWS research needs to more carefully consider the protonation state of potentially cooperative ligands.

AUTHOR INFORMATION

Corresponding Author

*E-mail: t@unt.edu.

Notes

The authors declare no competing financial interest.

ACKNOWLEDGMENTS

W.C.O. is a student in the Texas Academy of Math and Science (TAMS) program at the University of North Texas (UNT). W.C.O. thanks the TAMS Summer Research Fellowship for its support of this research. We acknowledge the NSF CCI Center for Enabling New Technologies through Catalysis (CENTC) for its support of this research (CHE-1205189). Numerous fruitful discussions with and suggestions from Prof. D. Michael Heinekey, Dr. Timothy P. Brewster (Department of Chemistry, University of Washington), and other CENTC collaborators are gratefully acknowledged.

REFERENCES

(1) Murahashi, S.; Naota, T.; Ito, K.; Maeda, Y.; Take, H. *J. Org. Chem.* **1987**, *52*, 4319−4327.

(2) Stanley, G. G.; Aubry, D. A.; Bridges, N.; Barker, B.; Courtney, B. *Prepr. Pap. Am. Chem. Soc., Div. Fuel Chem.* **2004**, *49*, 712−713.

(3) (a) Aubry, D. *Synthesis, Separation, and Reactivities of Multidentate Phosphine Ligands and Investigation into Dirhodium Hydroformylation and Hydroxycarboxylation Catalysis*. Ph. D. Dissertation, Louisiana State University, 2004. (b) Barnum, A. R. *Studies of a Dirhodium*

Tetraphosphine Catalyst for Hydroformylation and Aldehyde-Water Shift Catalysis. Ph. D. Dissertation, Louisiana State University, 2012.
(4) Carmo, M.; Fritz, D. L.; Mergel, J.; Stolten, D. *Int. J. Hydrogen Energy* **2013**, *38*, 4901−4934.
(5) Funk, J. E. *Int. J. Hydrogen Energy* **2001**, *26*, 185−190.
(6) Navarro, R. M.; del Valle, F.; Villoria de la Mano, J. A.; Álvarez-Galván, M. C.; Fierro, J. L. G. *Adv. Chem. Eng.* **2009**, *36*, 111−14310.1016/S0065-2377(09)00404-9
(7) Yamada, T.; Rhode, O.; Takai, T.; Mukaiyama, T. *Chem. Lett.* **1991**, *20*, 5−8.
(8) Rodríguez-Lugo, R. E.; Trincado, M.; Vogt, M.; Tewes, F.; Santiso-Quinones, G.; Grützmacher, H. *Nat. Chem.* **2013**, *5*, 342−347.
(9) Brewster, T. P.; Ou, W. C.; Tran, J. C.; Goldberg, K. I.; Hanson, S. K.; Cundari, T. R.; Heinekey, D. M. *ACS Catal.* **2014**, *4*, 3034−3038.
(10) Kawahara, R.; Fujita, K.; Yamaguchi, R. *J. Am. Chem. Soc.* **2012**, *134*, 3643−3646.
(11) Tundo, P.; Anastas, P.; Black, D. S.; Breen, J.; Collins, T.; Memoli, S.; Miyamoto, J.; Polyakoff, M.; Tumas, W. *Pure Appl. Chem.* **2000**, *72*, 1207−1228.
(12) Miller, A. J. M.; Heinekey, D. M.; Mayer, J. M.; Goldberg, K. I. *Angew. Chem., Int. Ed.* **2013**, *52*, 3981−3984.
(13) Frisch, M. J.; Trucks, G. W.; Schlegel, H. B.; Scuseria, G. E.; Robb, M. A.; Cheeseman, J. R.; Scalmani, G.; Barone, V.; Mennucci, B.; Petersson, G. A.; Nakatsuji, H.; Caricato, M.; Li, X.; Hratchian, H. P.; Izmaylov, A. F.; Bloino, J.; Zheng, G.; Sonnenberg, J. L.; Hada, M.; Ehara, M.; Toyota, K.; Fukuda, R.; Hasegawa, J.; Ishida, M.; Nakajima, T.; Honda, Y.; Kitao, O.; Nakai, H.; Vreven, T.; Montgomery, J. A., Jr.; Peralta, J. E.; Ogliaro, F.; Bearpark, M.; Heyd, J. J.; Brothers, E.; Kudin, K. N.; Staroverov, V. N.; Kobayashi, R.; Normand, J.; Raghavachari, K.; Rendell, A.; Burant, J. C.; Iyengar, S. S.; Tomasi, J.; Cossi, M.; Rega, N.; Millam, M. J.; Klene, M.; Knox, J. E.; Cross, J. B.; Bakken, V.; Adamo, C.; Jaramillo, J.; Gomperts, R.; Stratmann, R. E.; Yazyev, O.; Austin, A. J.; Cammi, R.; Pomelli, C.; Ochterski, J. W.; Martin, R. L.; Morokuma, K.; Zakrzewski, V. G.; Voth, G. A.; Salvador, P.; Dannenberg, J. J.; Dapprich, S.; Daniels, A. D.; Farkas, Ö.; Foresman, J. B.; Ortiz, J. V.; Cioslowski, J.; Fox, D. J. *Gaussian 09*, Revision D.01; Gaussian, Inc., Wallingford, CT, 2009.
(14) Adamo, C.; Barone, V. *J. Chem. Phys.* **1999**, *110*, 6158−6170.
(15) Andrae, D.; Haeussermann, U.; Dolg, M.; Stoll, H.; Preuss, H. *Theor. Chim. Acta.* **1990**, *77*, 123−141.
(16) Krishnan, R.; Binkley, J. S.; Seeger, R.; Pople, J. A. *J. Chem. Phys.* **1980**, *72*, 650−654.
(17) Campos, J.; Kundu, S.; Pahls, D. R.; Brookhart, M.; Carmona, E.; Cundari, T. R. *J. Am. Chem. Soc.* **2013**, *135*, 1217−1220.
(18) Marenich, A. V.; Cramer, C. J.; Truhlar, D. G. *J. Phys. Chem. B* **2009**, *113*, 6378−6396.
(19) Li, H.; Hall, M. B. *J. Am. Chem. Soc.* **2014**, *136*, 383−395.
(20) Yamakawa, M.; Ito, H.; Noyori, R. *J. Am. Chem. Soc.* **2000**, *122*, 1466−1478.
(21) Collaborative experimental efforts were focused on propionaldehyde, benzaldehyde, and acetaldehyde; the smallest of the three, acetaldehyde, was chosen for computational efficiency.
(22) A 20-electron isomer of complex **5** with acetic acid in the outer coordination sphere of Ir was found but was higher in energy by 1 kcal mol^{-1}. An 18-electron isomer of complex **5** with η^3-Cp* instead of η^6-Cp* was also found but was much higher in energy than presented complex **5** (∼30 kcal mol^{-1}).
(23) Hasanayn, F.; Baroudi, A. *Organometallics* **2013**, *32*, 2493−2496.
(24) Hasanayn, F.; Baroudi, A.; Bengali, A. A.; Goldman, A. S. *Organometallics* **2013**, *32*, 6969−6985.
(25) Nieto, I.; Livings, M. S.; Sacci, J. B., III; Reuther, L. E.; Zeller, M.; Papish, E. T. *Organometallics* **2011**, *30*, 6339−6342.